Resistivity and implantation distribution of hydrogen and helium in metals

1992 J. Phys.: Condens. Matter 4 9573

(http://iopscience.iop.org/0953-8984/4/48/012)

J. Phys.: Condens. Matter 4 (1992) 9573–9580. Printed in the UK

Resistivity and implantation distribution of hydrogen and helium in metals

A S Soltan†, P Jung and A A Gadallah†

Institut für Festkörperforschung, Association EURATOM-KFA, Forschungszentrum Jülich, D-5170 Jülich, Federal Republic of Germany

Received 16 March 1992, in final form 27 July 1992

Abstract. The resistivity contributions and the widths of the distributions of hydrogen and helium, implanted with energies from 0.125 to 3 keV at 5 K into thin film specimens of tantalum and rhenium, were obtained from resistivity damage rate measurements. The following values of the resistivity contribution per unit concentration of implanted atoms were derived: for tantalum $\rho_H \simeq 0.7 \pm 0.1$ $\mu\Omega$ m and $\rho_{He} \simeq 0.7 \pm 0.2$ $\mu\Omega$ m; for rhenium $\rho_H = 3.0 \pm 0.5$ $\mu\Omega$ m and $\rho_{He} = 6 \pm 1$ $\mu\Omega$ m. These values and data from other metals are related to the resistivities of defects and to thermal resistivities. The widths of the implantation distributions are compared with previous measurements on other metals and with Monte Carlo calculations.

1. Introduction

An investigation of the properties of hydrogen in some metals is complicated by low solubility and strong binding to vacancies, especially at lower temperatures. The same applies in all metals for noble gases like helium. Therefore, in order to investigate their properties in such metals, hydrogen or helium must be implanted, and implantation must be performed at energies below the threshold energy for defect production, to avoid the production of lattice defects. Even for heavy target elements, subthreshold implantation implies energies below about 0.5 keV for ^{4}He and below 1.5 keV for ^{1}H. Particles of such energies have ranges of only a few nm. On the other hand, for resistivity measurements coherent films are needed which only form at much higher thicknesses t. Therefore, the implantation will be inhomogeneous, i.e. the implanted region of an effective width w will be in parallel to an unimplanted region of width $t - w$. If for the sake of simplicity a homogeneous distribution is assumed in the implanted region, the measured resistivity damage $\Delta\rho$ is given by

$$\Delta\rho = \Delta\rho_i/[t/w + (t/w - 1)\Delta\rho_i/\rho_0] \tag{1}$$

where ρ_0 is the initial resistivity of the film and $\Delta\rho_i$ is the resistivity change in the implanted region. The measured resistivity damage rate $d\rho/d\phi$—resistivity change per particle fluence—is then given by

$$d\rho/d\phi = (d\rho_i/d\phi)(w/t)[1 - (t/w - 1)\,\Delta\rho/\rho_0]^2. \tag{2}$$

† Permanent address: Assiut University, Assiut, Egypt.

0953-8984/92/489573+08$07.50

For $w \ll t$ a square root dependence of $d\rho/d\phi$ on $\Delta\rho$ is obtained. For small damage, i.e. $\Delta\rho \ll \rho_0$, $d\rho/d\phi$ is reduced by a factor w/t compared with $d\rho_i/d\phi$ [1, 2]. $\Delta\rho_i$ consists of contributions from the implanted atoms (I) and from displaced lattice atoms (F):

$$\Delta\rho_i = \rho_I c_I + \rho_F c_F. \tag{3}$$

c_I and c_F are the atomic concentrations of implanted atoms and of displacement defects (Frenkel pairs). They are defined by $n_{I,F}/n_0$, where $n_{I,F,0}$ are the respective number densities of implanted atoms, defects and target atoms. ρ_I (I = H, D, He) and ρ_F are the resistivity contributions per unit concentration, i.e. $c_{I,F} = 1$. The damage rate can then be separated according to equation (3):

$$(d\rho/d\phi)(n_0 t/\rho_F) = \rho_I/\rho_F + c_F/c_I. \tag{4}$$

Equation (4) indicates that at energies below the threshold for defect production ($c_F = 0$) an energy-independent damage rate $d\rho/d\phi = \rho_I/n_0 t$ will be observed from which ρ_I can be obtained.

Equation (1) was derived under the assumption of a constant distribution in the implanted layer. If a more realistic distribution is used, numerical calculations are necessary instead of equation (2). For example, Monte Carlo simulations (TRIM [3]) give a Weibull distribution for low-energy-implanted light ions and an exponential distribution for the Frenkel defects [2]. From a fit of these distributions to the damage rate curves $d\rho/d\phi$ versus $\Delta\rho$, the resistivity contributions of implanted atoms and of defects can be separated and the widths w_I and w_F of their distributions are obtained. This separation is possible as w_I turns out to be much wider than w_F, in qualitative agreement with the TRIM calculations. In the case of defects a minor correction for defect saturation (cf [2]) must be considered. For this correction, recombination volumes (in units of atomic volumes) of 200 (Ta) and 300 (Re) have been used according to a compilation in [4]. It can be shown [2] that the results are rather insensitive to this value.

2. Experimental details

Thin films of thicknesses from 90 to 250 nm were produced by evaporation on sapphire holders, which were heated during evaporation to 1373 K for rhenium and to 1323 K for tantalum, respectively. The evaporation speed was about 0.2 nm s^{-1} and the vacuum pressure during evaporation was typically 10^{-5} Pa. The specimens were strongly textured with film normal directions of ⟨1320⟩ in rhenium and 5° off ⟨121⟩ in tantalum. With a molybdenum mask on the evaporation holder, specimens of 6 mm length and 1.5 mm width were shaped for four-wire resistance measurements. The residual-to-room-temperature resistivity ratios (RRR) after evaporation ranged from about 3 to 20. Attempts were made to increase the RRR (see table 1). Wrapping the evaporated films in zirconium foils and annealing them at 1400 K in evacuated quartz capsules increased the RRR only in some specimens. The best results were obtained by evaporating about 40 nm Zr onto the end pieces outside the gauge section of the specimens. This evaporation was done *in situ* immediately after the evaporation of the specimen material at a temperature of about 800 K. Secondary-ion mass spectroscopy

Table 1. Specimen, implantation and fit parameters from damage rate measurements (cf figure 1). The energies E in the table give the energy per implanted atom.

	Target			Implantation			Fit parameters			
	t (nm)	ρ_0 (nΩ m)	RRR	Ion	E (keV)	$(1-r/1+\gamma)$[a]	ρ_I ($\mu\Omega$ m/UC)	c_F/c_I	w_I (nm)	w_F (nm)
Re	166	23.7	9.0	D	0.2	0.381	1.21	0	9.5	—[b]
	205	51.8	4.7	D	1.5	0.394	3.26	0	62	—[b]
Re	151	49.5	4.8	He	0.3	0.319	1.54	0	5.5	—
	157	58.7	4.4	He	3.0	0.339	6.7	1.1	32.5	8
Ta	84	50.6	3.6	D	0.2	0.400	0.36	0	6	—
	85	48.2	3.7	D	1.5	0.417	0.77	0.12	27	5.5
Ta	178	13.9	10.7	He	0.3	0.313	0.58	0	11	—
	123	56.3	3.3	He	3.0	0.344	4.2[c]	0.75	21	7

[a] The backscattering coefficients r were derived from TRIM, while the secondary electron factor γ was taken from results on hydrogen in tungsten [10].

[b] The very short initial drop of damage rate is disregarded.

[c] This value is subject to a large error due to the relatively small resistivity contribution of the implanted atoms ($\rho_I \ll \rho_F$).

(SIMS) was used to determine the impurity content of some of the specimens. SIMS failed to give reliable contents of light impurities (H,O), but showed some relation between the RRR and the content of metallic impurities. Calculations showed that resistivity contributions from surface scattering (size effect) were negligible for the present specimens.

Specimen thicknesses were determined from the resistance geometry factor, given by the difference in room-temperature and helium resistance divided by the room-temperature resistivity ρ_{RT} of pure bulk material ($\rho_{RT} = 190\,n\Omega$ m for Re, $\rho_{RT} = 131\,n\Omega$ m for Ta). Surface profilometry (Dektak) confirmed these results within about 10%.

The specimens were mounted in a low-temperature implantation facility with a vacuum better than 10^{-7} mbar. During implantation the pressure rose to about 10^{-4} mbar due to the implantation gas from the ion source. The beam current was measured on the specimens. The implantation current was corrected by the backscattering factor r and the secondary electron emission factor γ in order to obtain the implantation dose. Values of total correction factors $(1-r)/(1+\gamma)$ are given in table 1. Contributions from recoil implantation of adsorbed atoms can be neglected. Details of the implantation procedure are given elsewhere [2, 6]. Some isochronal annealing experiments were performed after implantation to investigate the mobility of the implanted atoms [7].

3. Results

Figure 1 shows normalized damage rates of rhenium ($\rho_F = 22\ \mu\Omega$ m/UC) during implantation of deuterium and helium at different energies. At the beginning of deuterium implantation the damage rates drop sharply at very small doses by about 15%. Later on, the deuterium data as well as the helium data at lower energies follow

almost straight lines, whilst the 3 keV helium curve shows pronounced curvature. When the short initial drop of the deuterium data is disregarded, the data can be fitted (full curves) in analogy to equation (1) using a Weibull distribution for the implanted atoms and an exponential distribution for Frenkel pairs. The fitting parameters ρ_I, c_F/c_I, w_I and w_F are given in table 1. Initial damage rates of rhenium as a function of energy are shown in figure 2. The normalized deuterium damage rates show specimen-to-specimen variations of more than a factor of two and are generally higher than those of hydrogen. In contrast with previous results on platinum [1], and on gold and tungsten [2], the hydrogen and especially the deuterium damage rates show an energy dependence for subthreshold ($E \leqslant E_d$) implantation. The energy dependence of the helium data at subthreshold energies is smaller.

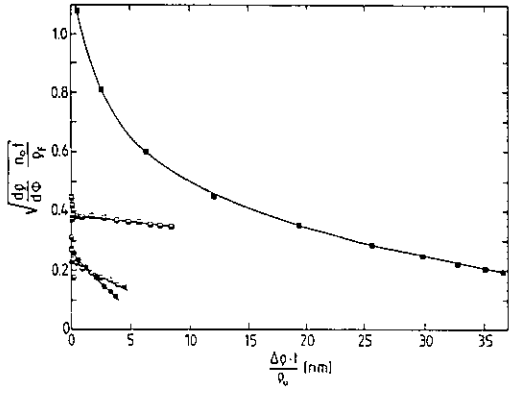

Figure 1. Normalized damage rates as function of normalized damage in rhenium during implantation of D and He. Energies and specimen thicknesses were: D, 0.2 keV, 166 nm (◒); 1.5 keV, 205 nm (◒); He, 0.3 keV, 151 nm (●); 3 keV, 157 nm (■). The size effect correction ($l/\rho_b = 6 \times 10^{-16}$ Ω m^2) was negligible. The full curves are fits to the data, with the parameters given in table 1.

The energies E_d in figures 2 and 3 are derived from threshold energies (44 eV for Re, 32 eV for Ta, for data compilation see [4]) from electron irradiations. The present investigations show for the first time experimentally that the onset of defect production during ion implantation is in good agreement with these values.

Normalized damage rate curves for implantation of deuterium and helium in tantalum ($\rho_F = 17$ μΩ m/UC) show the same qualitative features as in the case of rhenium, except for the initial 15% drop of the Re(D) data. Figure 3 shows normalized damage rates of Ta as a function of energy. As in the case of rhenium, the damage rates of hydrogen and deuterium implantation show significant energy dependences at subthreshold energies ($E \leqslant E_d$), but in agreement with equation (4) only a weak energy dependence of the damage rates of subthreshold helium implantation.

4. Discussion

The relatively low RRR values indicate rather high levels of lattice imperfection in both metals. Imperfections may be dislocations from thermal stresses or more probably gaseous impurities. For example, a typical value of 5 μΩ m/UC for the resistivity contribution of dissolved gas atoms in tantalum gives a lower limit of the impurity concentrations in the 10^{-3} range. At this level impurities will probably influence neither the stopping of the implanted ions nor the production of lattice defects, nor

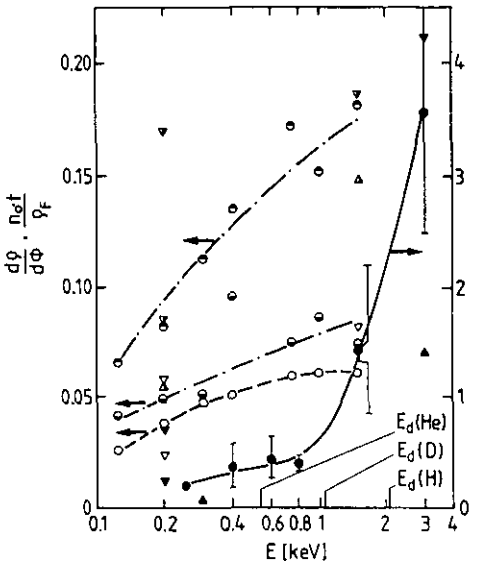

Figure 2. Normalized damage rates as a function of energy per atom for implantation of hydrogen (empty symbols, broken curve), deuterium (half-full symbols, chain curves) and helium (full symbols, full curve) in rhenium. The triangles show results from figure 1 (▲, ▲) and from damage rate measurements before annealing (▽, ▼, ▼), respectively. The E_d values on the abscissa indicate the threshold energies for irradiation with the respective ions.

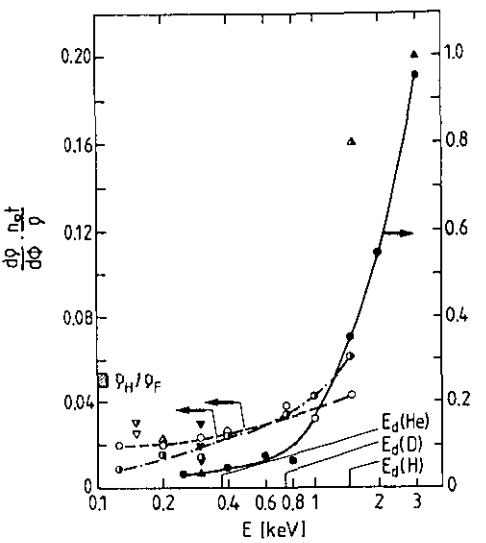

Figure 3. Normalized damage rates as a function of energy per atom for implantation of hydrogen (empty symbols, broken curve), deuterium (half-full symbols, chain curve) and helium (full symbols, full curve) in tantalum. The triangles show results from damage rate curves (▲, ▲) and from damage rate measurements before annealing (▽, ▼, ▼), respectively., The E_d values on the abscissa indicate the threshold energies for irradiation with the respective ions. On the ordinate the range of ρ_H/ρ_F from the literature [11] is indicated.

ρ_I and ρ_F. On the other hand, impurities may trap migrating atoms or defects, when these become mobile.

The energy dependence of the damage rates at subthreshold energies (figures 2 and 3) for hydrogen and deuterium implantation in rhenium and tantalum is in contradiction with equation (4). This may indicate some mobility and losses to the surface already during the rather shallow implantation. This supposition is corroborated in the case of tantalum by the annealing experiments which show some resistivity recovery already during hydrogen and deuterium implantation [7]. On the other hand, in the case of rhenium after D implantation, a first small recovery step is only observed at 40 K. If nevertheless $\rho_{H,D}$ values are extracted according to equation (4) these will represent only lower limits. At $E \simeq E_d$ the following values are obtained: 1.4–3 $\mu\Omega$ m/UC for rhenium and 0.7 $\mu\Omega$ m/UC for tantalum. These values are in rough agreement with the values obtained from the normalized damage rates (cf figure 1 and table 1). Also, in these experiments the results from low-energy implantation give probably too low values. The ρ_H value for tantalum from figure 3 also agrees reasonably with the data from normalized damage rates (table 1) and also matches exactly a value of 0.71 ± 0.01 $\mu\Omega$ m reported for dissolved H and D [8].

For helium, ρ_{He} values $\sim 6 \pm 2$ (Re) and $\sim 0.7 \pm 0.2$ $\mu\Omega$ m (Ta) are obtained from the damage rates at $E \simeq E_d$ in figures 2 and 3 while the fits to the damage

rate curves (cf figure 1, see table 1) give values in this range but with large scatter. As in the case of deuterium, implantation at lower energies gives lower ρ_{He} values. The annealing experiments show recovery after helium implantation only above 20 K (Ta) and 300 K (Re), respectively.

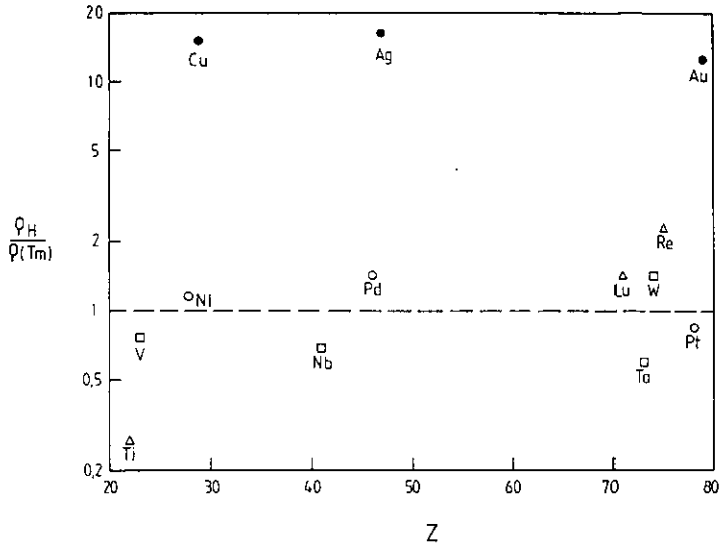

Figure 4. Ratios of hydrogen resistivities per unit concentration to resistivities at the melting point as a function of atomic number Z. Data are from table 2 and from [11, 12]. Different symbols indicate FCC (○, ●), BCC (□) and HCP (△) metals. Temperatures for ρ_H of metals not cited in table 2 are: Ti, 1177 K; V, 469 K and Pd, 443 K. Ratios of other rare earths [11] approach the lutetium value ($Z = 71$).

In table 2 the resistivity contributions from implanted hydrogen and helium in various metals are compared with values of Frenkel defects. For all metals $\rho_H \leqslant \rho_{He} \leqslant \rho_F$ is fulfilled within experimental error. Two other features of the data in table 2 and figure 4 are striking.

(i) ρ_H equals the resistivity at the melting point $\rho(T_m)$ within a factor of about two, except for β-titanium and for the noble metals Cu, Ag and Au, for which $\rho_H/\rho(T_m) \simeq 15$ is obtained (see figure 4). As for most metals the Frenkel pair resistivity ρ_F is also proportional to $\rho(T_m)$, $\rho_F/\rho(T_m) \simeq 18$ [9], the relations $\rho_H/\rho_F \simeq 0.055$ for non-noble metals and $\rho_H/\rho_F \simeq 0.83$ for noble metals are obtained.

(ii) Relations for ρ_{He} exist neither with ρ_F nor with $\rho(T_m)$. For FCC and HCP metals almost constant ρ_{He} values of 3.2 ± 1.5 (FCC) and ~ 6 $\mu\Omega$ m/UC (HCP) are obtained, while for BCC metals the ρ_{He} values range from 0.7 to 7.6 $\mu\Omega$ m/UC.

As described above, fits of equation (2) to the damage rate curves (cf figure 1) also yield effective widths of the distributions of implanted atoms and Frenkel defects. In figure 5 the data (cf table 1) are compared with results on gold and tungsten [2] and with Monte Carlo calculations (TRIM [3]). The major results of this comparison are as follows.

(i) The width of deuterium implanted in rhenium is in the same range as that

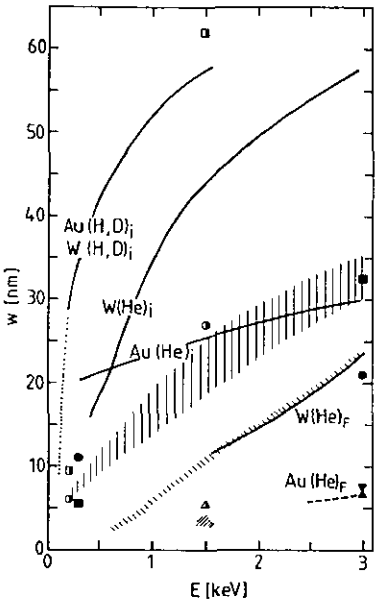

Figure 5. Widths of the distributions of implanted atoms (○, □) and of defects (△, ▽) in tantalum (○, △) and rhenium (□, ▽) as a function of energy per atom. Symbols indicate deuterium (half-full) and helium (full) implantation, respectively. The curves represent implanted atoms (i) and defects (F) from a previous study [2] on gold (Au) and tungsten (W). The shaded areas indicate TRIM calculations [2, 3] for H, D and He in Au, W, Ta and Re (|||), for vacancies produced during He implantation (\\\), and for defects produced during deuterium implantation (///), respectively.

Table 2. A comparison of resistivity contributions per unit concentration ($\mu\Omega$ m/UC) of hydrogen[a], helium and Frenkel pairs[b] and resistivity ($\mu\Omega$ m) at the melting point[c] in metals.

Metal		ρ_H	ρ_{He}	ρ_F	$\rho(T_m)$
FCC	Au	1.7 ± 0.5 [2]	3.3 ± 0.8 [2]	2.5	0.136
	Cu	1.50 [11]	1.7 [d]	2.4	0.10
	Ni	0.67 [11]	3.0 [d]	7.1	0.59
	Pt	0.5 [1]	4.8 [1]	9.5	0.60
BCC	Nb	0.63 [8]	2.03 [15]	16	0.93
	Ta	0.7 ± 0.1 [e]	0.7 ± 0.2	17	1.18
	W	1.6 ± 0.2 [2]	7.6 ± 0.6 [2]	27	1.14
HCP	Lu	2.9 [13]	5.8 [13]	75	2.06
	Re	3.0 ± 0.5	6 ± 1	22	1.32

[a] ρ_H values correspond to liquid-helium temperature.
[b] Most ρ_F values ($\mu\Omega$ m/UC) are taken from a compilation in [4]. ρ_{He} and ρ_F values correspond to liquid-helium temperature, except for Cu, Ni[d] and Nb (469 K).
[c] $\rho(T_m)$ data ($\mu\Omega$ m) are extrapolated from [12].
[d] Values obtained after room-temperature implantation at high energies, i.e. the values correspond to substitutional helium [14].
[e] Measurements of thermally dissolved hydrogen above room temperature yield 0.71 ± 0.01 [8].

of hydrogen and deuterium implanted into gold and tungsten [2], and is much larger than predicted by TRIM.

(ii) The width of deuterium implanted with 1.5 keV into tantalum is much smaller than in the other metals and agrees reasonably with the TRIM calculations.

(iii) The widths of helium distributions in rhenium agree with the results for He

in Au [2] and fall within the range of TRIM calculations, while the width of helium in tantalum at 3 keV is somewhat lower.

(iv) The widths of the defect distributions produced by 3 keV helium implantation in Re and Ta agree with that for He in Au but are much smaller than that in tungsten and are also smaller than predicted by TRIM.

Acknowledgments

The authors are indebted to F Römer and H J Bierfeld for their help in specimen preparation, to S Mantl for TRIM calculations, to R Vaßen for contributions to the tantalum measurements, to H Klein for technical assistance, and to H Hammelrath from RWTH Aachen for texture analysis. The work of ASS at Jülich was supported by the CHANNEL between the Federal Republic of Germany and the Arabic Republic of Egypt.

References

[1] Vassen R and Jung P 1988 *Phys. Rev.* B **37** 2911
[2] Jung P and Soltan A S 1991 *Radiat. Eff. Defects Solids* **118** 309
[3] Biersack J P and Haggmark L G 1980 *Nucl. Instrum. Methods* **174** 257
[4] Jung P 1991 *Atomic Defects in Metals (Landolt–Börnstein New Series, Group III)* vol 25, p 1
[5] Soltan A S, Vaßen R and Jung P 1991 *J. Appl. Phys.* **70** 793
[6] Vaßen R 1986 *Diplomarbeit* Rheinisch-Westfälische Technische Hochschule Aachen, Federal Republic of Germany
[7] Soltan A S 1990 *PhD Thesis* Assiut University, Egypt
[8] Watanabe K and Fukai Y 1980 *J. Phys. F: Met. Phys.* **10** 1795
[9] Jung P 1980 *Radiat. Eff.* **51** 249
[10] Mahadevan P 1965 *Phys. Rev.* **140** 1407
[11] Papastaikoudis C, Lengeler B and Jäger W 1983 *J. Phys. F: Met. Phys.* **13** 2257
[12] Bass J 1982 *Metals: Electronic Transport Phenomena (Landolt–Börnstein New Series, Group III)* vol 15a, p 1
[13] Jung P and Lässer R 1988 *Phys. Rev.* B **37** 2844
[14] Gaber A 1983 *Report KFA Jülich* JÜL-1860 (ISSN 0366-0885)
[15] Chen C G and Birnbaum H K 1979 *J. Nucl. Mater.* **79** 128